Electrolyte effects on the electrochemical performance of microemulsions

Jing Peng[a*], Ye Xiao[a], Adam Imel[b], Brian Andrew Barth[b], Nelly M. Cantillo[b], K. McKensie Nelms[c], and Thomas A. Zawodzinski[b,d**]

a. School of Materials Science and Engineering, Beihang University, Beijing, 100191 P. R. China

b. Department of Chemical & Biomolecular Engineering, University of Tennessee, Knoxville, Tennessee 37996, USA

c. Department of Biosystems Engineering & Soil Science, The University of Tennessee, Knoxville, Tennessee 37996, USA

d. Physical Chemistry of Materials Group, Oak Ridge National Laboratory, Oak Ridge, Tennessee 37831, USA

* Corresponding author: pengj@buaa.edu.cn

** Co-corresponding author: tzawodzi@utk.edu

Abstract

We report a study of the electrochemistry of Ferrocene (Fc) in a Tween®20 (polyethylene glycol (20) sorbitan monolaurate) /1-butanol/ water/Toluene (TBWT) microemulsion system, focusing on the effects of electrolyte components. Resistance and conductivity measurements are used along with Cyclic Voltammetry (CV) to

characterize the effects of supporting electrolyte, such as Bu_4NBF_4 and KNO_3, on the electrochemical performance and transport properties of Fc. With increasing Fc-containing oil phase concentration in the microemulsion, the observed peak current density fails to increase proportionately with the Fc concentration. Adding 0.05m Bu_4NBF_4 in the oil phase significantly increases the current density, presumably by lowering the resistance of microemulsion nonpolar phase and promoting the accessibility of Fc in the system. Moreover, increasing the aqueous phase supporting electrolyte from 0.5m KNO_3 to 1m KNO_3 does not exhibit an analogous effect. We discuss these results in the context of our working hypothesis for microemulsion organization and its implications for electron transfer to Fc.

Keyword: Microemulsion; Supporting electrolyte; Electrochemical performance; Conductivity

1. Introduction

Redox flow batteries (RFBs) are currently attracting considerable attention due to their promising application as stationary large-scale electrochemical energy storage devices. As secondary batteries, RFBs have some significant advantages, such as decoupling between energy storage and power delivery, flexibility and scalability, long cycle life, high efficiency, safe and clean. The RFBs could reduce the burden of power output at the consumption peaks. This function is extremely important for developing smart grids and distributed generation stations. Moreover, RFBs are able to convert and store electricity in the range of several kW/kW h up to tens of MW/MW h[1, 2], therefore, they are capable of delivering stable and flexible

electricity to some important departments, such as hospital and airport, to ensure their smooth operation.

In the past few decades, many studies on RFBs have focused on aqueous electrolytes, which offer advantages of high ionic conductivity, low cost and excellent system reliability[3-5]. Among them, the vanadium redox flow batteries (VRFBs) are the most studied flow battery. Significant efforts and progress have been made to improve the cell current density and power density of VRFBs. Nevertheless, VRFBs based on aqueous electrolytes have limited energy density of 25 Wh L^{-1}, significantly lower than that of the lithium ion battery[6, 7], due to the narrow electrochemical window (1.23V) and low concentration of redox species[8, 9]. In this regard, employing nonaqueous electrolyte solutions is another strategy for improving the performance of RFBs. The organic solvents in nonaqueous electrolytes could simultaneously provide a larger electrochemical window than that associated with aqueous electrolytes as well as higher solubility and a wider range of redox couples[10]. These advantages could potentially lead to a higher cell voltage and energy density in RFBs. However, the fact is that the performance of nonaqueous RFBs still cannot compete with the typical aqueous RFBs due to the low ionic conductivity of nonaqueous electrolytes, even though sometimes the solubility of redox couple can be much higher than the 2M of vanadium salt in VRFBs, i.e. 4M naphthene in 1,2-dimethoxyethane[11], 9.7M biphenyl in N,N-dimethylformamide and 3M octafluoronaphthalene in propylene carbonate[12].

The respective advantageous features of aqueous and nonaqueous electrolytes

inspired us to study its application of microemulsion systems in RFBs. Perhaps we can decouple solubility and conductivity in the electrolytes. Microemulsions are a class of thermodynamically stable isotropic dispersions of two or more immiscible liquids, which are stabilized by the surfactant film at the interface between the liquids. They are widely investigated in the field of synthesis, drug delivery, chemical reaction and separation[13-17]. Conventional microemulsions are composed of water, oil and surfactant, and are classified as water-in-oil (W/O), bicontinuous, and oil-in-water (O/W), depending on their compositions. The immiscibility of the water and oil phases provides a possible way to decouple one solvent (i.e. water), which supports the high ionic conductivity of electrolytes, from another solvent (i.e. oil phase), which could provide high solubility of redox couples. Therefore, the special properties of microemulsions seem to provide a new strategy to develop the electrolytes of RFBs. Redox couples are dissolved in the oil phase, while the water phase, with low viscosity and high ionic conductivity, forms a bicontinuous, fluid structure with the oil phase, enabling transport of both redox species and charged ions. With this, it is possible to use redox couples with high potential or solubility or with unique functionality in the oil phase of the electrolytes but still achieve much higher ionic conductivity than in organic solvents, thereby developing RFBs with high energy and power density.

One concern is that the electrochemical window of microemulsion is still limited to 1.23V due to the presence of water. However, there are two studies which suggest that this is not the case. Ying[18] and Iwunze[19] reported results for

TX-100/H_2O/1-butyl-3-methylomodazolium hexafluorophosphate ($bmimPF_6$) and didodecyldimethylammonium bromide/H_2O/dodecane microemulsions, respectively, with electrochemical windows about 2.6V, similar to the electrochemical window of the oil phase in these systems, with only slightly variation depending on the compositions of microemulsions. These two reports strongly suggest that high potentials can be accessed in microemulsion electrolytes.

Previously, we reported some initial studies of the electrochemical performance of the typical redox species, ferrocene(Fc) in a Tween®20/1-butanol/H_2O /toluene (TBWT) microemulsion system[20] and speculated on the applicability of microemulsions in redox flow batteries. In this microemulsion, Tween®20 and 1-butanol function as the surfactant and cosurfactant, respectively, while toluene is the solvent for redox-active species and water is used as the conductive medium. This microemulsion exhibits a considerable oil uptake, as high as 58 wt.% at some specific water/surfactant ratios. The high oil uptake implies that we can achieve a high overall loading of oil-soluble electroactive compounds in the overall solution. Fc exhibits acceptable electrochemical reversibility over a wide range of compositions. In addition, the conductivity of the TBWT microemulsion could be flexibly tuned by changing compositions.

Here we report more studies in this TBWT microemulsion system with Fc dissolved in oil phase. In addition to reporting a broader range of data, we probe the effect of adding an oil phase-soluble supporting electrolyte salt. We further analyze diffusion in this broader range of composition, comparing it to preliminary data

obtained with pulsed field gradient Nuclear Magnetic Resonance (PFG NMR) methods.

2. Experimental

2.1 Microemulsion Preparation

Tween®20 (polyethylene glycol (20) sorbitan monolaurate, Sigma-Aldrich) and 1-butanol (purity>99%, Sigma-Aldrich) were used as surfactant and cosurfactant, respectively. The weight ratio of Tween®20 and 1-butanol was set to 82.5 wt%/17.5 wt% for all samples in order to achieve the highest oil uptake as discussed in our previous report[20]. The surfactant and cosurfactant mixture with this fixed weight ratio are represented as "S" in this work. Toluene (HPLC grade, Fisher Scientific) and deionized water (18.2 MΩ cm^{-1}) were used as the oil phase (O) and the water phase (W), respectively. The composition of the microemulsion is given as S/W/O in some of the plots, representing the weight percentage ratios of each component over the whole microemulsion. In addition, we use $(S/W)_{0.4/0.6}$ to represent samples with weight ratio of surfactant to water equals to 0.4/0.6, but the oil content varies.

The surfactant and cosurfactant mixture "S" was mixed with KNO_3 (purity >99%, Fisher Scientific) aqueous solution as the starting materials with certain weight ratio of S/W. The vials containing S and W were stirred at 1200 rpm at 20°C by placing them on a temperature controlled stirring plate. A given amount of toluene solution with Fc (Purity>98%, Fisher Scientific) and Bu_4NBF_4 (BNF) (purity >99%, Fisher Scientific) was added into the vials and kept stirring for 5 mins until all components were well mixed. The composition of microemulsion samples studied in this work

were all chosen within the 2-phase boundary as shown in our previous report[20].

2.2 Cyclic Voltammetry Measurements

Cyclic voltammetry (CV) measurements were performed on a Bio-Logic SP-200 potentiostat at 20±0.5°C. The electrochemical measurements were conducted using a three-electrode configuration, with a glassy carbon working electrode, a saturated calomel (SCE) reference electrode and a Pt wire counter electrode. A Teflon™ cap with three holes was used to cover the cell. The spacing between adjacent electrodes was set by placing each of them in a fixed hole and inserting them through the cap. Approximately, 10 mL of microemulsion was used for each measurement. Before each measurement, the working electrode was polished using 0.05 μm aluminum oxide slurries and then washed carefully with distilled water. The experiments were carried out under a nitrogen atmosphere to avoid the effect of oxygen. All CV data was iR corrected taking into account the solution resistance. Measurements at four scan rates, i.e. 0.01 $V \cdot s^{-1}$, 0.025$V \cdot s^{-1}$, 0.05$V \cdot s^{-1}$ and 0.1$V \cdot s^{-1}$, were performed for each sample to calculate diffusion coefficients.

2.3 Conductivity Measurements

The conductivity was measured by a YSI 3200 conductivity meter at 20°C±0.5°C. About 20 mL solutions were stirred in vials placed on a temperature controlled stirring plate. A certain amount of toluene was added into the solution and kept stirring for 5 mins before the conductivity measurement. The increments of the volume of toluene added into vials were set to 10μL, 50μL or 100μL, respectively, depending on the scale of maximum oil uptake in systems with different

compositions.

2.4 NMR Measurements

The microemulsion samples were packed into 5 mm NMR tube. ^{19}F NMR were characterized with CCl_3F in CH_3OH (0ppm) as ^{19}F reference. The CCl_3F in CH_3OH were packed in insert with 2mm diameter, which are placed in a 5 mm NMR tube to avoid interaction between the sample and reference. PFG NMR measurements were carried out on an AVANCE III HD 400 MHz NMR spectrometer using a broad band probe equipped with a 60 G/cm gradient coil at 20˚C. A DOSY bipolar pulse pair stimulated echo pulse sequence was used to measure ^1H diffusion coefficient for characterizing the mobility of Fc. The gradient strengths were arrayed in 16 values with linear increment for each experiment, and the diffusion coefficient data *D* can be extracted by fitting the raw data using Stejskal-Tanner equation:[21, 22]

$$I = I_0 * e^{-D(\gamma\ g\ \delta)^2\ \left(\Delta - \frac{\delta}{3}\right)} \qquad (1)$$

Where *I* is the signal strength observed with applied gradient *g* (0-60 G/cm), I_0 is the signal in absence of the field gradient, $\gamma$is gyromagnetic ratio of the studied nucleus, δ is the gradient pulse duration and Δ is the diffusion delay.

2.5 Chronocoulometry measurement

Chronocoulometry measurements were performed using a Bio-Logic SP-200 potentiostat equipped with a low current probe at room temperature. Ten milliliters of sample were added to a glass vial fit with a Teflon stopper, through which three electrodes were inserted into the solution–a glassy carbon working electrode, a saturated calomel reference electrode, and a Pt wire counter electrode. The sample

was purged with nitrogen prior to data collection. Chronocoulometry measurements were performed in quintuplicate using an applied potential of 0.7V vs. SCE (after iR compensation at 85% of the high frequency resistance) for 30 seconds. The solution was stirred between trials to ensure consistent initial conditions for each trial. The microemulsion that was used for this measurement was 5 wt % oil phase with 0.5m (mol/kg) Fc, 55 wt% 0.5m KNO_3 (aq), and 40 wt% Tween 20/1-butanol (82.5%/17.5%, by mass) microemulsion, by volume. The resulting microemulsion was 25mM Fc overall.

3. Results and Discussion

To investigate the reversibility and stabilization of electrochemical materials in microemulsions, a typical redox species, Fc, was applied in our system as a probe. Three series of microemulsions with different Fc concentrations (0.1m, 0.5m and 0.985m in toluene) were prepared for $(S/W)_{0.4/0.6}$ and $(S/W)_{0.5/0.5}$. Figure 1(a) shows the voltammogram of Fc in the $(S/W)_{0.4/0.6}$ with 5wt% oil phase(O), exhibiting the typical of electrochemically reversible behavior. In addition, the voltammogram of Fc in system of $(S/W)_{0.4/0.6}$ and $(S/W)_{0.5/0.5}$ with various composition are plotted in Figure S1 and Figure S2, respectively. The peak separations (ΔEs) of TBWT microemulsion are listed in Table S1. ΔEs in system of $(S/W)_{0.4/0.6}$ are 58-70 mV, which suggests reasonable reversibility of Fc in the microemulsion, but ΔE increases at the higher oil phase(O) uptake. This phenomenon is even more obvious in the case of $(S/W)_{0.5/0.5}$ with high Fc concentration. Under conditions of high surfactant and high oil concentration, the voltammogram is controlled by the kinetics of the redox reaction

because either the ion transfer reaction or electron transfer reaction becoming slower could result in wider peak separation[23].

The peak current density obtained for TBWT microemulsion with three different Fc concentrations as a function of oil weight percentage have been plotted in Figure 1(b) and Figure 1(c). The ratio of oxidation peak current density (i_{op}) of microemulsions with various Fc concentrations to i_{op}(0.1 m Fc in Toluene) as a function of oil weight percentage are plotted in Figure 2. The ratio of i_{op}(0.5 m Fc in toluene)/i_{op}(0.1 m Fc in toluene) is about 3-4.5, which is smaller than the ratio of Fc concentrations in the two samples. The ratio is even smaller for i_{op}(0.985 m Fc in toluene)/i_{op}(0.1 m Fc in toluene) as compared to the ratio of Fc concentration, i.e. 0.985m/0.1m=9.85, especially in the system of $(S/W)_{0.5/0.5}$. In that case the current densities of samples with 0.985m Fc in toluene only show a slightly higher value than the samples with 0.5 m Fc.

One possible cause of this would be increasing resistance with the increase of Fc concentration. The solution resistance is listed in Table S2. Changes in resistance appear to be modest with slight trends across the composition range. Another possibility is that accessible Fc is present in the surfactant layer, a hypothesis that we proposed in our previous report, may also cause this phenomenon[20].

The main point of our earlier hypothesis is that the Fc is present in the nonpolar tail groups of Tween®20. With no toluene in the micelle, Tween®20 can solubilize roughly 2 wt% of ferrocene. Upon oxidation, the Fc^+ can remain in the interior of the surfactant assembly. This creates proximity to compensating ionic motion coupled to

the redox process, thereby maintaining local electroneutrality during the electron transfer reaction. When the concentration of Fc increases, i.e. 0.1m, 0.5m to 0.985m, the capability of gathering Fc is limited by the number of tail groups available in the whole microemulsion system, possibly limiting the efficiency of chemical reaction in TBWT microemulsion at the higher Fc concentration[24]. This is likely due to structural changes. Not only does the S/W ratio change the structure but so does the O/W ratio.

The CV characterization was performed at four different scan rates, from which the apparent diffusion coefficient(*D*) of Fc in a quasi-reversible reaction can be calculated using the Randles-Sevcik equation[25-27] (2).

$$i_p = 0.436nFAC(nFvD/RT)^{1/2} \qquad (2)$$

Where ip is the peak current density, n is the number of electrons transferred in the electrochemical reaction (n=1 for the Fc); A is the electrode area (0.07065 cm^2 for the glassy carbon); D is the diffusion coefficient of Fc; C is the concentration of Fc; T is the temperature in K; and ν is the scan rate. The Randles-Sevcik equation as used here can be applied to obtain the diffusion coefficient of Fc in a quasi-reversible system. However this equation is only an approximation, and therefore does not yield an exact value, unlike the case of chronocoulometry.

Through use of Chronocoulometry, diffusivity can be calculated using the Cottrell equation under the assumption ferrocene concentration at the surface of the working electrode is approximately zero. The time-integrated from of the Cottrell equation is:

$$Q = 2nFAC\pi^{-1/2}D^{1/2}t^{1/2} \qquad (3)$$

where Q is the total charge due to the faradaic process, t is time, and n, F, A, and C have their usual meaning, as previously mentioned. The mean ferrocene diffusivity was 3.96×10^{-7} cm^2/s with a standard deviation of 9.39×10^{-9} cm^2/s; this agrees with diffusivity obtained using cyclic voltammetry for similar microemulsions.

The D(Fc) is plotted as a function of oil weight percentage in Figure 3. The calculated D(Fc) results are on the order of 10^{-8} to 10^{-6} $cm^2\ s^{-1}$. D(Fc) in TBWT microemulsion with the higher Fc concentration is generally an order of magnitude lower than those at a lower Fc concentration. Generally, $D(\mathrm{Fc})_{(S/W)_{0.4/0.6}}$ decreases as the oil weight percentage increases, but $D(\mathrm{Fc})_{(S/W)_{0.5/0.5}}$ shows only a slightly change while the toluene fraction is smaller than 15 wt.%. To better understand the trend of D(Fc) with water content, the D(Fc) is also plotted as a function of water phase volume fraction in Figure S3.

At first glance, diffusion of the ferrocene occurs simply through the oil phase of the bicontinuous mixture and it is perhaps surprising that it decreases with increasing oil content. Naturally, there is a certain average tortuosity associated with diffusion that does not exist in the simple solution. This evokes a picture of diffusion in a sinuous tube. In this circumstance, the local (or micro-) viscosity of the fluid is the controlling factor and increasing oil content would seem to allow a larger solvent regime in which Fc can diffuse. In addition, we must also take into account the probable interaction of ferrocene itself with the hydrophobic tail of the surfactant. Indeed, we have previously interpreted the relatively rapid electrode kinetics of ferrocene oxidation as indicative of such an interaction and we know that Fc is soluble in the surfactant

itself. Again, we would expect the introduction of increased oil to increase the overall fluidity of the contained fluid. This, however, is contrary to the observed results.

Diffusion in the microemulsion is likely to be a complicated function of composition. A number of aspects can have an impact on the mass transfer process. First, the structure of the microemulsion itself has an influence. Though we have shown that the gross structure of the microemulsion is comprised of bicontinuous hydrophilic and hydrophobic phase in the composition range considered here, the addition of oil to a surfactant/water mixture changes the structure and behavior of the surfactant layer. The oil-free structure is essentially micellar and highly fluid, with well hydrated head groups. As oil is added, the surfactant is distended and its physical properties change. For example, the radius of curvature is altered to accommodate the oil and the layer necessarily stiffens. Stiffening of head groups, one could argue, negatively impacts the fluidity of the Fc that is present in the surfactant phase. However, the effect of increasing oil doesn't lower $D(\mathrm{Fc})_{(\mathrm{S/W})_{0.5/0.5}}$ as it does in $D(\mathrm{Fc})_{(\mathrm{S/W})_{0.4/0.6}}$. $D(\mathrm{Fc})_{(\mathrm{S/W})_{0.5/0.5}}$ with less water content tends to transit as more W/O-like microemulsion, therefore increasing oil lead to more (or larger) oil channels connected with Fc diffusion facilitated, which trades off the surface pressure effect.

In addition, our small-angle neutron scattering (SANS) study proves that $(\mathrm{S/W})_{0.4/0.6}$ shows a most ordered bicontinuous structure than the others, and the ordering at the surfactant-solvent interface results in a stiffer interface[28]. A considerable proportion of Fc delivered in the redox mechanism can be hindered in $(\mathrm{S/W})_{0.4/0.6}$ due to the stiffer interface while they are diffusing across the surfactant

interface, then resulting in $D(\mathrm{Fc})_{(\mathrm{S/W})_{0.4/0.6}} < D(\mathrm{Fc})_{(\mathrm{S/W})_{0.5/0.5}}$. The Randles–Sevcik equations are only an approximation, and therefore do not represent an exact value. To obtain a more fine-grained picture, we have used PFG NMR and chronocoulometry experiments to determine the diffusion coefficient of various components of the system in this composition range. It's found that D(Fc) extracted from the CV measurements are very close to both NMR and chronocoulometry results.

To evaluate the limit of reversibility, cyclic voltammetry at scan rate up to 22 $\mathrm{V \cdot s^{-1}}$ have been reported in our previous work[20]. The resulting voltammogram evinced a fast electron transfer through the boundaries of the oil phase. In this work, we worked on studying the reversibility for couple of different microemulsion samples. An example of voltammograms as a function of scan rate is plotted in Figure S4. Plots of the peak current density vs. the square root of the scan rate is shown in Figure 4. A good fit to Eq. 2 can be obtained at scan rates up to 4 $\mathrm{V \cdot s^{-1}}$ for microemulsion with S/W/O=38.6/58.0/3.4 wt% in Figure 4(a), exhibiting a significant deviation from linearity at higher scan rates. This upper reversibility limit, however, is greatly influenced by the composition of the system, as shown in Figure 4(a)-4(c) for different Toluene concentration in $(\mathrm{S/W})_{0.4/0.6}$ and in Figure S5 for different S/W ratios at low toluene content. In Figure 4a, 3.4 wt. % Toluene concentration in $(\mathrm{S/W})_{0.4/0.6}$ exhibits a linear behavior through the entire scan rate range, while higher toluene concentrations (11.0 and 16.2 wt. %) undergo the transition to quasireversibility at scan rates as low as 1 $\mathrm{V \cdot s^{-1}}$. Quasireversible behavior implies that the electron transfer

rates are lower than the rate of mass transport. This is as reported in reference 20.

As in our previous work and following we use the method reported by Nicholson[29] and Lavagnini, et al[30] for the evaluation of kinetic parameter k^0. This requires the fitting ΔE to a working curve to obtain values of a function ψ defined in Eq. 4. The evaluation of k^0 by Nicholson's method applies to the range of peak separation between 57 and 250 mV, during which the electrode process is progressing from reversible to irreversible[31].

$$\psi = k^0[\pi DnFv/RT]^{-\frac{1}{2}} \qquad (4)$$

The ψ is calculated from Eq. 5:

$$\psi = (-0.6288 + 0.0021X)/(1 - 0.0017X) \qquad (5)$$

Where X stands for $\Delta E_P \times n$, in mV; ΔE_P is the peak separation in CV curves; D is the diffusion coefficient of the electroactive species, n is the number of electrons transferred in the electrochemical reaction, F is the Faraday constant, v is the scan rate; R is the molar gas constant, and T is the absolute temperature.

This method was used to evaluate the rate constant of k^0 for the samples shown in Figure 4b-4c and Figure S5b, which are typical quasi-reversible reaction process. The plots of ψ *versus* $[\pi DnFv/(RT)]^{-1/2}$ for these samples are shown in Figure S6. The heterogeneous rate constants calculated for these samples are listed in Table 1. The values are generally in the order of 10^{-3} cm s^{-1}, which are about one third of the results, 5.9×10^{-3} cm s^{-1}, for the sample with composition of 58.1/36.9/5.0 wt% reported in our previous work[20]. The reason for lower heterogeneous rate constants of these samples can be ascribed to two possible effects: increased oil concentration in sample 4b and 4c

and increased surfactant weight percentage in Figure S5b. They both come down to increased resistance in microemulsion systems.

Table 1. Diffusion coefficient and heterogeneous rate constants at 20˚C.

Sample #	Composition S/W/O (w/w/w%)	C(Fc) (mol cm^{-3})	D^0 (cm^2 s^{-1})	k^0 (cm s^{-1})
4b	35.6/53.4/11	5.68×10^{-5}	4.21×10^{-8}	1.4×10^{-3}
4c	33.5/50.3/16.2	8.93×10^{-5}	4.27×10^{-8}	1.5×10^{-3}
S5b	47.9/47.9/4.2	2.0×10^{-5}	1.57×10^{-7}	2.0×10^{-3}

As electrolyte is needed to achieve adequate conductivity for efficient use in a cell, discerning how the addition of supporting electrolyte affects the electrochemical reaction and transport of Fc in the microemulsion is also very important for developing the microemulsion electrolytes for flow cell applications. In addition to bulk effects associated with a device, the electrochemical reaction requires that charged ions can effectively migrate and compensate for changes in the charge state of the redox active species in the microemulsions[32]. Bard's group showed that this can lead to loss of electrochemical activity in droplets in surfactant-free emulsions. In that case, the electrochemical activity depended on the ability of ions to enter or leave the emulsion droplet. We previously suggested that the microemulsion case may behave differently since (mobile) ions in the aqueous phase can be present within a short distance of active species (here Fc/Fc^+) in the nonpolar phase[20]. It is also known that ions can move back and forth across the surfactant boundary as they undergo redox processes that sufficiently change their polarity, and indeed,

cross-phase exchange can be rapid on the experimental time scale[20].

To further probe the ion transport requirements for electrochemistry in microemulsions, we studied effects of two supporting electrolytes, such as BNF and KNO_3. More specifically, the following supporting electrolyte combinations used were: i) 0.5 m KNO_3 as an aqueous supporting electrolyte in systems with and without 0.05m BNF dissolved in the oil phase; and ii) 0.05m BNF was initially dissolved in the oil phase, with varied KNO_3 concentration.

Representative CVs of Fc in the electrolyte with and without 0.05m BNF are shown in Figure 5 along with plots of the peak current density for Fc in a TBWT microemulsion with and without 0.05 m BNF supporting electrolyte as a function of oil weight percentage (Figure S7), with 0.5m Fc in the oil. The compositions for the CV characterization were chosen based on the phase boundary determination reported in our previous work[20]. As we expected, the phase boundary observed for microemulsions with BNF didn't deviate significantly as compared with the ones without BNF, due to the low concentration, i.e. 0.05m, and low hydrophobicity of BNF[33]. Due to the limitation of maximum oil uptake, the microemulsion with the higher water content can only take up less than 5 wt.% of oil for the samples $(S/W)_{0.1/0.9}$ to $(S/W)_{0.3/0.7}$ and the current densities of these samples are much lower than those for the microemulsions with $(S/W)_{0.5/0.5}$ and $(S/W)_{0.6/0.4}$. The samples with BNF show a higher peak current density than those without BNF for the samples with high water content, i.e. $(S/W)_{0.1/0.9}$ and $(S/W)_{0.2/0.8}$. The peak current density is not affected by the presence of BNF at higher water content. The peak current density is

plotted as a function of water phase volume fraction in Figure S8.

A comparison of D(Fc) calculated from CV results between the TBWT microemulsions with and without BNF as supporting electrolyte is shown in Figure 6. The D(Fc) of the samples with BNF are generally higher than those without BNF at the high water volume fraction range though only slightly so in the low water content range, as one might expect from the data of Figure S7.

The conductivity of samples with $(S/W)_{0.5/0.5}$ in Figure S9 shows a lightly higher value in samples with BNF than the ones without BNF. As reported in Table S3 for the two series of microemulsion, the resistance of the samples without added BNF is roughly 2 times higher than that with 0.05m BNF supporting electrolyte at S/W≤0.3/0.7, but the resistance in these two series of samples only shows a slightly difference when S/W is higher. Therefore, the trends of D(Fc) and resistance are broadly similar, the *diametric opposite* of the expected result for a viscosity-controlled effect (i.e. lower viscosity leads to higher D and higher σ, or lower resistance). In addition, BNF, one of quaternary ammonium compounds, acts as a phase-transfer catalyst in the two-phase reaction. Open chain PEO compounds, i.e. Tween®20 in microemulsion, often give a crown ether effect, i.e. increase phase contact and may constitute practically alternative phase transfer agents. It's reported that the combination of microemulsion with some phase-transfer reagent can dramatically increase the reaction rate[34].

To further explore the contribution of BNF and determine its location in microemulsion, ^{19}F NMR were performed on BNF in H_2O, toluene, Tween®

20/1-butanol and TBWT microemulsion with chemical shift of -150.5ppm, -149.1ppm, -151.1 and -150.2ppm, respectively, as shown in Figure 7. The ^{19}F NMR of BF_4^- ions in the microemulsion shows a small shift of 0.3 ppm to the one in H_2O, which suggests a similar chemical environment of BF_4^- ions in both solutions and hence strongly suggests that the location of BF_4^- ions is in the water phase of microemulsion[33]. With the evidence shown above, it should be noted that even though the BNF was dissolved in the oil phase initially, it still transferred into water phase due to low transfer energy of tetrabutylammonium ions, i.e. -7.7 kJ/mol[35]. In other words, the BNF in microemulsion actually act as a supporting electrolyte in the water phase..

The concentration of supporting electrolyte in the aqueous phase was also varied in this work. For each sample with a specific S/W ratio, one composition within the phase boundary was characterized by CV, with different concentrations of supporting electrolyte in aqueous phase, i.e. 0.5m KNO_3 and 1m KNO_3, respectively, as shown in Figure 7 and Figure S10. The peak current density of the sample with 1m KNO_3 in the water phase is lower than that with 0.5m KNO_3 at the lowest water contents. The ΔE suggests reasonable reversibility for the Fc in the microemulsion with lower S/W ratio, but ΔE significantly increases as the water content is reduced, especially in the system with only 0.5m KNO_3. The effect of increased concentration appears to be to reduce ΔE. Table S4 shows the increasing KNO_3 concentration reduced the resistance of the microemulsion solution at all water contents. Isono[36] reported that the conductivity $\sigma(1m) = 1.76\sigma(0.5m)$ for aqueous KNO_3 solutions. This is in exact agreement with the

ratio observed for high water content samples a to c in Table S4. Therefore, the conductivity of these samples indicates that they behave as aqueous solutions. The ratio is slightly higher, approaching 2 but varying somewhat, for the remaining samples. One plausible explanation is that a fraction of the KNO_3 interacts with the surfactant head groups; in the 1m solutions, this partitioning leaves a greater concentration of salt in the fluid phase.

The calculated *D*(Fc) in TBWT microemulsion with 0.5m and 1m KNO_3 aqueous supporting electrolyte have been plotted in Figure 9a. The numbers shown in the figure are the oil wt% in the microemulsion. Values of *D*(Fc) for all samples with 1m KNO_3 in water phase are lower than those for 0.5m KNO_3 solutions. Unsurprisingly, this result agrees well with the behavior of the peak current density observed in Figure 8. The lower current density and *D*(Fc) in 1m KNO_3 system suggest a higher viscosity in 1m KNO_3 than 0.5m KNO_3 but the viscosity of aqueous KNO_3 solutions does not change much in this composition range. At the high water content range (S/W=0.1/0.9 to 0.3/0.7), *D*(Fc) decreases as the water content drops. However, the latter 3 points were obtained with different oil contents as the maximum possible oil content is lower when the surfactant content is low. Still, the *D*(Fc) peaks at ~ 50 vol% of water and appears to tend to decrease sharply after this peak.

The conductivity of TBWT microemulsions with different KNO_3 concentration is shown in Figure 9b as a function of water phase volume fraction. In these samples, the supporting electrolyte in the oil phase was 0.05m BNF for all samples and the supporting electrolyte concentration in the aqueous phase was either 0.5m or 1m

KNO_3. The conductivity increases from ~5×10^{-2} mS cm^{-1} to 80 mS cm^{-1} as the water phase volume fraction changes from 8 V% to 92V%, and it slightly decreases with increasing oil weight fraction as shown in Figure S11. Over the entire composition range, the conductivity of the TBWT microemulsions with 1m KNO_3 is always higher than those with 0.05m KNO_3 when they are compared at the same surfactant/oil/water composition. The overall trend is readily understood as resulting from the significant decrease in the water phase volume fraction available as a conducting phase.

To develop a more nuanced picture of the behavior of these electrolytes, we now discuss the results in an integrated fashion. The primary results are:

i) $D(\mathrm{Fc})_{(S/W)_{0.5/0.5}}$ is higher than $D(\mathrm{Fc})_{(S/W)_{0.4/0.6}}$; by adding supporting electrolytes BNF in the oil phase, the diffusivity of Fc has been promoted, i.e. $D(\mathrm{Fc})_{0.05\mathrm{m\ BNF}} > D(\mathrm{Fc})_{\mathrm{No\ BNF}}$; in addition, the more concentrated aqueous phase with 1m KNO_3 could have generally slowed down the diffusion coefficient of Fc, i.e. $D(\mathrm{Fc})_{1\mathrm{m\ KNO_3}} < D(\mathrm{Fc})_{0.5\mathrm{m\ KNO_3}}$.

ii) The conductivity of TBWT raises as the concentration of supporting electrolyte KNO_3 in the aqueous phase increases from 0.5m to 1m.

Combining the CV, D(Fc) and conductivity results, it is found that even though the conductivity can be increased by raising the concentration of KNO_3, the diffusion of Fc^+ is a key step which suppresses the electrochemical performance of TBWT microemulsion with a higher KNO_3 concentration.

Based on our SANS studies, the microemulsion structure changes substantially over this range of composition[28]. However, by observing the samples with the same

oil content, ~8.1wt%, S/W=0.4/0.6 to 0.2/0.8, the trends of D(Fc) in samples with 0.5m and 1m KNO_3 do not simply follow the trend of the resistance, but exhibit an initial increase followed by a decrease after reaching a maximum around S/W=0.6/0.4, which evidence significant structure evolution within this range. A ternary blend of polystyrene (PS) and polyethylene oxide (PEO) homopolymers and a diblock copolymer PS-block-PEO acting as a surfactant with added salt LiTFSI form bicontinuous structures similar to TBWT microemulsions[28]. SANS on the PS/PEO/PS-block-PEO system showed that doubling the concentration of the salt produced a stiffer interface and even though the general bicontinuous structure was maintained the system became more segregated, similar to swollen lamellae[37]. Conductivity experiments show that the higher salt concentration actually lowers the ionic conductivity. Given the boundaries are stiffer in the lamellar structure this hinders ion transport while the bicontinuous structure increases the ion transport due to an increase in flexibility.

This phenomenon can be explained by the hypothesis we proposed in the previous work[20]. As the surfactant monolayers in microemulsion stabilized two phases with the polar end interacting with aqueous phase and the nonpolar end interacting with oil phase, the multiple polyethylene oxide (PEO) oligomers region consisted in Tween® 20 are likely to dissolve salt (KNO_3) in aqueous phase, while the nonpolar accommodate Fc, keeping it within the surfactant. With that, ions can be expected to readily move in and out of the palisade layer. Perhaps it is because of this special mechanism, due to the limited surfactant, especially in the microemulsion with low

surfactant content, it is possible that the accessibility of Fc is limited during the CV measurements, therefore the microemulsion systems with much higher KNO_3 concentration don't exhibit much superior electrochemical performance than the lower one.

Based on the discussion above, the ion transfer mechanism of the microemulsion electrolyte can be summarized. We suggested a mechanism of ion transfer associated with the electron transfer in which both halves of the active couple remain associated with the interphase surfactant region. In that case, a relatively minor process of transfer of NO3- anions in and out of this interphase region, which contains components of the aqueous phase and the oil phase in close proximity, would maintain electroneutrality. This seems plausible based on the relatively facile kinetics observed. However, at this point there is insufficient evidence to rule out the possible transfer of Fc+ into the aqueous phase upon oxidation of Fc.[20]

4. Conclusion

In this work, various concentration of Fc, and the supporting electrolytes, i.e. BNF and KNO_3, of TBWT microemulsion were studied by characterizing the CV, diffusion coefficient of Fc, resistance and conductivity. The results suggest that the electrochemical performance of microemulsion electrolyte doesn't follow to the general law of regular aqueous electrolytes and nonaqueous electrolytes, i.e. increasing concentration of redox active species, supporting electrolytes are not the direct and only parameter for adjusting the electrochemical performance of microemulsion. It's found that the limited coordination group, EO, in the surfactant of

microemulsion could significantly affect the current density and diffusion coefficient of Fc. We speculate that this work would help us to better understand the electrochemical mechanism in microemulsion system, and expand the choices of electrolytes in RFBs.

Acknowledgement

This work was supported as part of the Breakthrough Electrolytes for Energy Storage (BEES), an Energy Frontier Research Center funded by the U.S. Department of Energy, Office of Science, Basic Energy Sciences under Award # DE-SC0019409.

Conflicts of interest

There are no conflicts to declare.

References:

[1] P. Leung, X. Li, C.P. De León, L. Berlouis, C.J. Low, F.C. Walsh, Progress in redox flow batteries, remaining challenges and their applications in energy storage, Rsc Adv, 2 (2012) 10125-10156.

[2] C. Ponce de León, A. Frías-Ferrer, J. González-García, D.A. Szánto, F.C. Walsh, Redox flow cells for energy conversion, J Power Sources, 160 (2006) 716-732.

[3] W. Wang, Q. Luo, B. Li, X. Wei, L. Li, Z. Yang, Recent progress in redox flow battery research and development, Advanced Functional Materials, 23 (2013) 970-986.

[4] M. Ulaganathan, V. Aravindan, Q. Yan, S. Madhavi, M. Skyllas-Kazacos, T.M. Lim, Recent advancements in all-vanadium redox flow batteries, Advanced Materials Interfaces, 3 (2016) 1500309.

[5] J. Winsberg, T. Hagemann, T. Janoschka, M.D. Hager, U.S. Schubert, Redox-Flow Batteries: From Metals to Organic Redox-Active Materials, Angew. Chem.-Int. Edit., 56 (2017) 686-711.

[6] R. Ye, D. Henkensmeier, S.J. Yoon, Z. Huang, D.K. Kim, Z. Chang, S. Kim, R. Chen, Redox Flow Batteries for Energy Storage: A Technology Review, Journal of Electrochemical Energy Conversion and Storage, 15 (2017) 010801-010801-010821.

[7] M.A. Hannan, M.S.H. Lipu, A. Hussain, A. Mohamed, A review of lithium-ion battery state of charge estimation and management system in electric vehicle

applications: Challenges and recommendations, Renewable and Sustainable Energy Reviews, 78 (2017) 834-854.

[8] L. Joerissen, J. Garche, C. Fabjan, G. Tomazic, Possible use of vanadium redox-flow batteries for energy storage in small grids and stand-alone photovoltaic systems, J Power Sources, 127 (2004) 98-104.

[9] L. Cao, M. Skyllas-Kazacos, C. Menictas, J. Noack, A review of electrolyte additives and impurities in vanadium redox flow batteries, Journal of Energy Chemistry, 27 (2018) 1269-1291.

[10] P. Leung, A. Shah, L. Sanz, C. Flox, J. Morante, Q. Xu, M. Mohamed, C.P. de León, F. Walsh, Recent developments in organic redox flow batteries: a critical review, J Power Sources, 360 (2017) 243-283.

[11] G. Wang, B. Huang, D. Liu, D. Zheng, J. Harris, J. Xue, D. Qu, Exploring polycyclic aromatic hydrocarbons as an anolyte for nonaqueous redox flow batteries, J Mater Chem A, 6 (2018) 13286-13293.

[12] K. Gong, Q. Fang, S. Gu, S.F.Y. Li, Y. Yan, Nonaqueous redox-flow batteries: organic solvents, supporting electrolytes, and redox pairs, Energy & Environmental Science, 8 (2015) 3515-3530.

[13] M. Spiro, D.M. de Jesus, Nanoparticle catalysis in microemulsions: oxidation of n, n-dimethyl-p-phenylenediamine by cobalt (III) pentaammine chloride catalyzed by colloidal palladium in water/AOT/n-heptane microemulsions, Langmuir, 16 (2000) 2464-2468.

[14] C.J. Campbell, C.K. Njue, B. Nuthakki, J.F. Rusling, Influence of thickness on catalytic efficiency of cobalt corrin-polyion scaffolds on electrodes in microemulsions, Langmuir, 17 (2001) 3447-3453.

[15] F. Gao, C.-C. Ho, C.C. Co, Sugar-based microemulsion glass templates, Journal of the American Chemical Society, 126 (2004) 12746-12747.

[16] M. Summers, J. Eastoe, S. Davis, Formation of BaSO4 nanoparticles in microemulsions with polymerized surfactant shells, Langmuir, 18 (2002) 5023-5026.

[17] F.-F. Lv, L.-Q. Zheng, C.-H. Tung, Phase behavior of the microemulsions and the stability of the chloramphenicol in the microemulsion-based ocular drug delivery system, International journal of pharmaceutics, 301 (2005) 237-246.

[18] X. Ying, H. Zhou, J. Hu, Y. Xu, J. Zeng, J. Chen, Y. Kuang, Electrochemical behavior of K4Fe(CN)(6) in bmim PF6/TX-100/H2O based microemulsions, Journal of Applied Electrochemistry, 39 (2009) 1273-1278.

[19] M.O. Iwunze, A. Sucheta, J.F. Rusling, Bicontinuous microemulsions as media for electrochemical studies, Analytical chemistry, 62 (1990) 644-649.

[20] J. Peng, N.M. Cantillo, K.M. Nelms, L.S. Roberts, G. Goenaga, A. Imel, B.A. Barth, M. Dadmun, L. Heroux, D.G. Hayes, T. Zawodzinski, Electron Transfer in Microemulsion-Based Electrolytes, Acs Appl Mater Inter, 12 (2020) 40213-40219.

[21] D. Sinnaeve, The Stejskal–Tanner equation generalized for any gradient shape—an overview of most pulse sequences measuring free diffusion, Concepts in Magnetic Resonance Part A, 40A (2012) 39-65.

[22] E.O. Stejskal, J.E. Tanner, Spin diffusion measurements: spin echoes in the presence of a time-dependent field gradient, The journal of chemical physics, 42

(1965) 288-292.

[23] C. Liu, P. Peljo, X. Huang, W. Cheng, L. Wang, H. Deng, Single Organic Droplet Collision Voltammogram via Electron Transfer Coupled Ion Transfer, Analytical Chemistry, 89 (2017) 9284-9291.

[24] R.A. Mackay, S.A. Myers, L. Bodalbhai, A. Brajter-Toth, Microemulsion structure and its effect on electrochemical reactions, Analytical chemistry, 62 (1990) 1084-1090.

[25] P. Zanello, Inorganic electrochemistry: theory, practice and application, Royal Society of Chemistry2007.

[26] A. García-Miranda Ferrari, C.W. Foster, P.J. Kelly, D.A.C. Brownson, C.E. Banks, Determination of the Electrochemical Area of Screen-Printed Electrochemical Sensing Platforms, 8 (2018) 53.

[27] D. Brownson, C.E. Banks, The Handbook of Graphene Electrochemistry, Springer London2014.

[28] A. Imel, B. Barth, D.G. Hayes, M. Dadmun, T.A. Zawodzinski Jr, Microemulsions stabilized by the non-ionic surfactant polysorbate-20 – A small-angle neutron scattering study of

the bicontinuous phase evolution, Langmuir, Under review (2021).

[29] R.S. Nicholson, Theory and Application of Cyclic Voltammetry for Measurement of Electrode Reaction Kinetics, Analytical Chemistry, 37 (1965) 1351-1355.

[30] I. Lavagnini, R. Antiochia, F. Magno, An extended method for the practical evaluation of the standard rate constant from cyclic voltammetric data, Electroanalysis, 16 (2004) 505-506.

[31] R.J. Klingler, J.K. Kochi, Electron-transfer kinetics from cyclic voltammetry. Quantitative description of electrochemical reversibility, The Journal of Physical Chemistry, 85 (1981) 1731-1741.

[32] H. Deng, J.E. Dick, S. Kummer, U. Kragl, S.H. Strauss, A.J. Bard, Probing Ion Transfer across Liquid-Liquid Interfaces by Monitoring Collisions of Single Femtoliter Oil Droplets on Ultramicroelectrodes, Analytical Chemistry, 88 (2016) 7754-7761.

[33] C. Johans, M.A. Behrens, K.E. Bergquist, U. Olsson, J.A. Manzanares, Potential Determining Salts in Microemulsions: Interfacial Distribution and Effect on the Phase Behavior, Langmuir, 29 (2013) 15738-15746.

[34] B. Kronberg, B. Lindman, Surfactants and polymers in aqueous solution, John Wiley & Sons Ltd., Chichester2003.

[35] M. Kasuno, Y. Matsuyama, M. Iijima, Voltammetry of Ion Transfer at a Water–Toluene Micro- Interface, ChemElectroChem, 3 (2016) 694-697.

[36] T. Isono, Density, viscosity, and electrolytic conductivity of concentrated aqueous electrolyte solutions at several temperatures. Alkaline-earth chlorides, lanthanum chloride, sodium chloride, sodium nitrate, sodium bromide, potassium nitrate, potassium bromide, and cadmium nitrate, J Chem Eng Data, 29 (1984) 45-52.

[37] S. Xie, D.J. Meyer, E. Wang, F.S. Bates, T.P. Lodge, Structure and Properties of Bicontinuous Microemulsions from Salt-Doped Ternary Polymer Blends,

Macromolecules, 52 (2019) 9693-9702.

Figures:

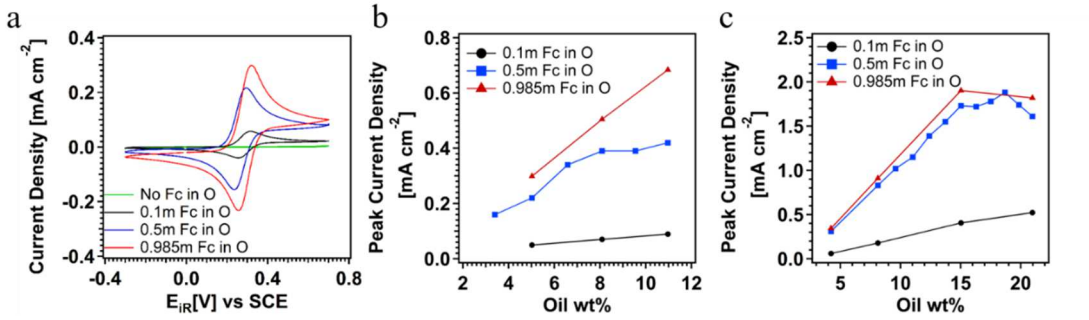

Figure 1. (a) Cyclic voltammogram of $(S/W)_{0.4/0.6}$ with 5 wt% of toluene with different Fc concentrations at scan rate of 0.01V s^{-1}; the current density as a function of oil weight percentage at scan rate of 0.01V s^{-1} for $(S/W)_{0.4/0.6}$ (b) and $(S/W)_{0.5/0.5}$ (c) with various Fc concentrations. (Experimental condition: 0.5 m KNO_3 in H_2O, no BNF in toluene; Working electrode: glassy carbon (3mm diameter, 0.07065 cm^2); counter electrode: Pt wire; Reference electrode: Saturated Calomel.)

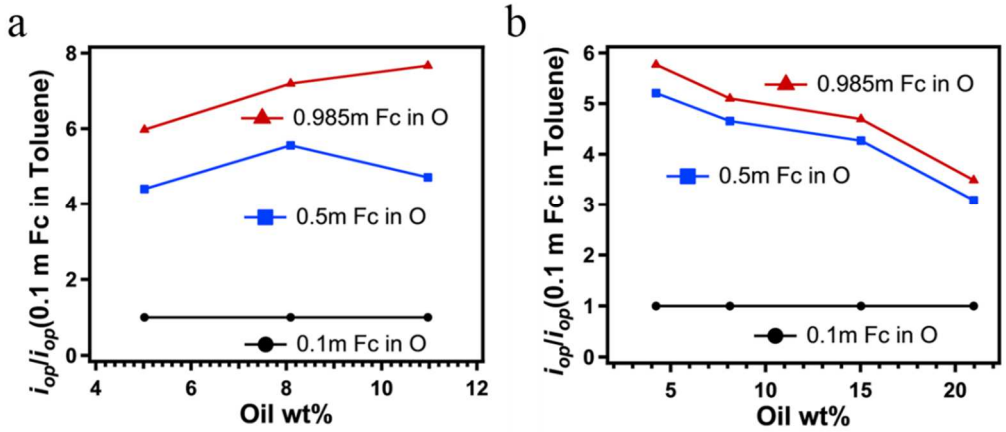

Figure 2. The ratio of i_{op}/i_{op}(0.1 m Fc in toluene) as a function of oil weight percentage for (a) $(S/W)_{0.4/0.6}$ and (b) $(S/W)_{0.5/0.5}$ with various Fc concentrations. (Experimental conditions are as in Figure 1.)

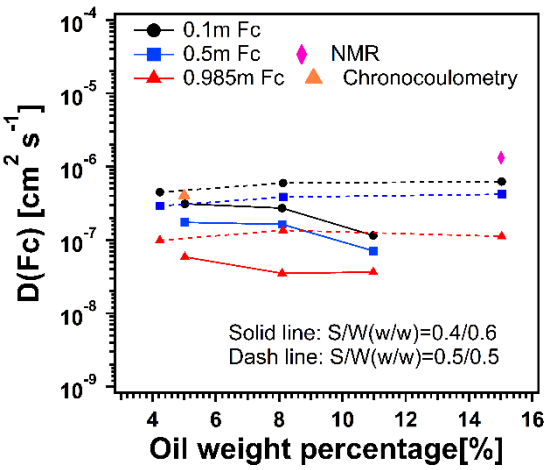

Figure 3. The diffusion coefficient of Fc in $(S/W)_{0.4/0.6}$ and $(S/W)_{0.5/0.5}$ with different Fc concentration as a function of oil weight percentage, in which the pink diamond shows the D(Fc) of 0.1m Fc in $(S/W)_{0.5/0.5}$ with 15 wt.% oil determined by NMR, and the orange triangle shows the D(Fc) of 0.5m Fc in $(S/W)_{0.42/0.58}$ with 5 wt.% oil determined by chronocoulometry. (0.5 m KNO_3 in H_2O, no BNF in Toluene; other experimental conditions are as in Figure 1.)

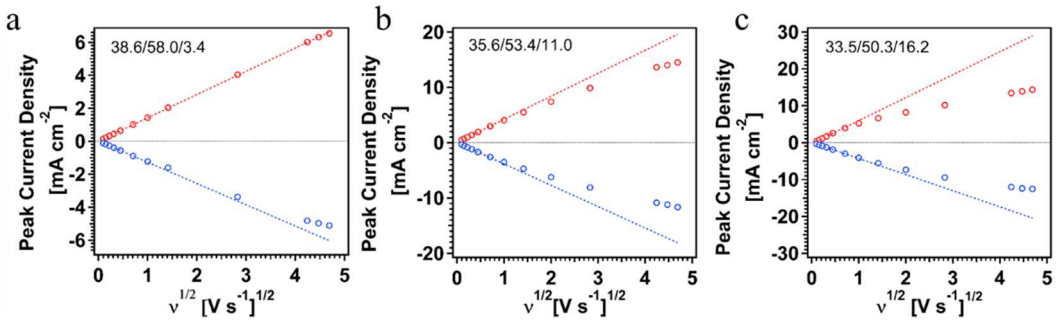

Figure 4. Plot of peak current density vs. square root of the scan rate for $(S/W)_{0.4/0.6}$ with 0.5m Fc concentration and S/W/O wt% shown in the figure. (Experimental conditions are as in Figure 1. In each case the S/W ratio is fixed at 0.4/0.6.)

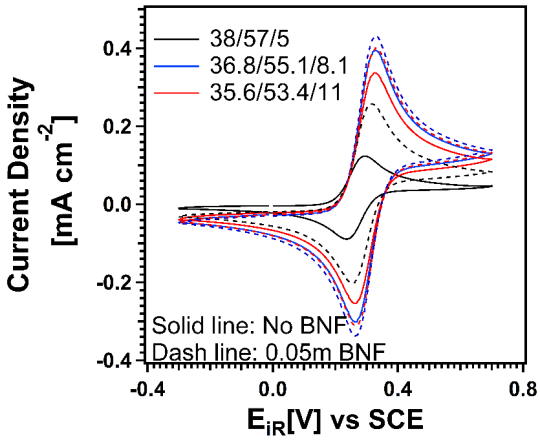

Figure 5. The comparison of cyclic voltammogram between the samples with 0.05 m BNF and without BNF as oil phase supporting electrolyte at scan rate of 0.01 V s^{-1}. (Experimental condition: $(S/W)_{0.4/0.6}$, 0.5m Fc in Toluene, 0.5 m KNO_3 in H_2O; other experimental conditions are as in Figure 1.)

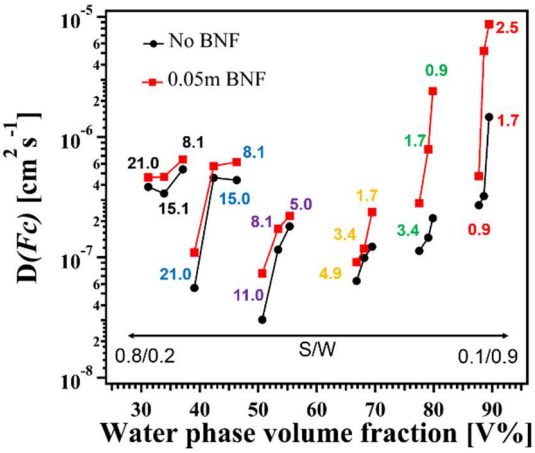

Figure 6. The comparison of *D*(Fc) of systems with and without BNF as supporting electrolyte in the oil phase as a function of water phase volume fraction at scan rate of 0.01 V s^{-1}. (The numbers shown in the figure are the oil weight percentage in different systems: $(S/W)_{0.1/0.9}$ (red); $(S/W)_{0.2/0.8}$ (green); $(S/W)_{0.3/0.7}$ (orange); $(S/W)_{0.4/0.6}$ (purple); $(S/W)_{0.5/0.5}$ (blue); and $(S/W)_{0.6/0.4}$ (black). (Experimental condition: 0.5 m KNO_3 in H_2O; other experimental conditions are as in Figure 1.)

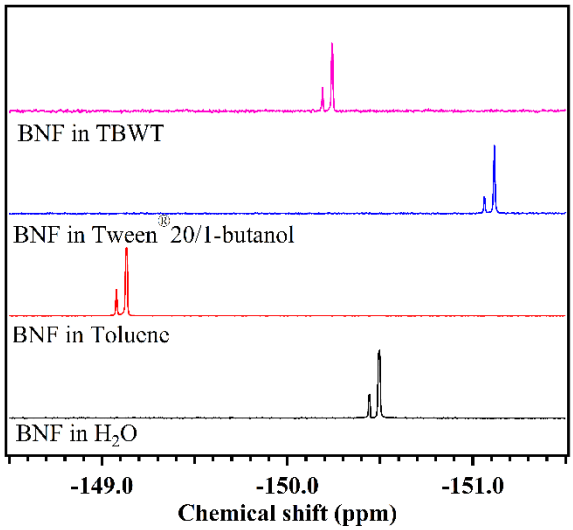

Figure 7. Normalized ^{19}F NMR lineshape of BNF in H_2O, Toluene, Tween®20/1-butanol and TBWT microemulsion (S/W/O=36.8/55.1/8.1 wt%).

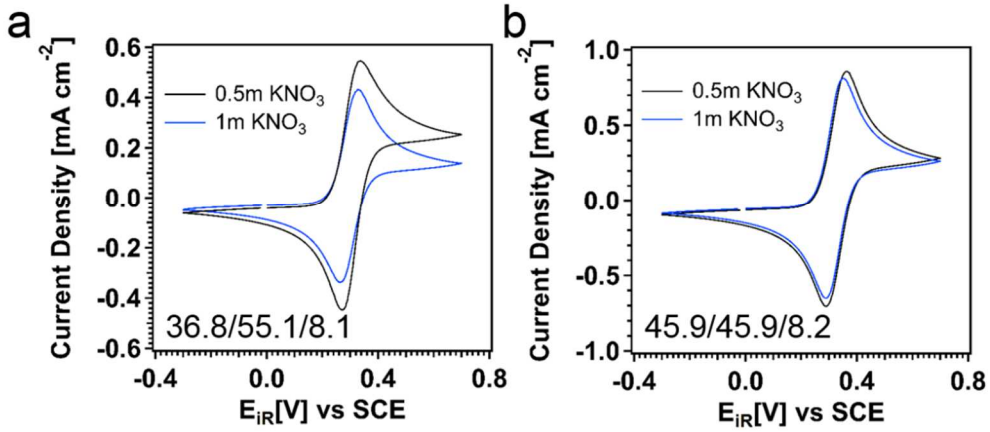

Figure 8. Cyclic voltammogram of microemulsion $(S/W)_{0.4/0.6}$ (a) and $(S/W)_{0.5/0.5}$ (b) with different KNO_3 concentration in the water phase at scan rate of 0.01 V s^{-1}. (Experimental conditions: 0.05 m BNF and 0.5m Fc in Toluene; 0.5m or 1m KNO_3 in H_2O; other experimental conditions are as in Figure 1.)

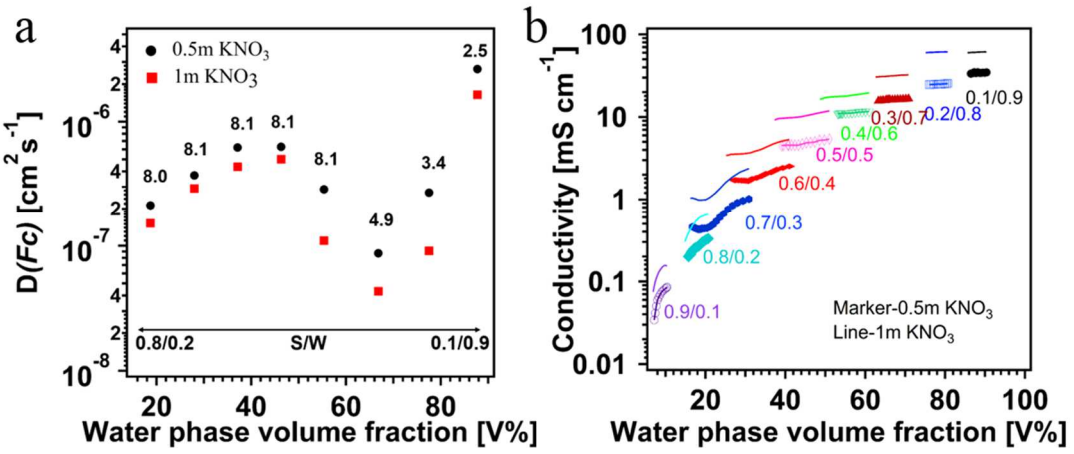

Figure 9. (a) The *D*(Fc) in systems with different KNO_3 concentration in the water phase as a function of water phase volume fraction. (The numbers shown on the top of data points in the figure are the oil weight percentage in different systems: from right to left: $(S/W)_{0.1/0.9}$, $(S/W)_{0.2/0.8}$, $(S/W)_{0.3/0.7}$, $(S/W)_{0.4/0.6}$, $(S/W)_{0.5/0.5}$, $(S/W)_{0.6/0.4}$, $(S/W)_{0.7/0.3}$ and $(S/W)_{0.8/0.2}$; (b) The conductivity of microemulsion with different KNO_3 concentration in the water phase as a function of water phase volume fraction (Points with the same colors are data for samples with the same S/W ratios but various oil wt%.). (Experimental condition: 0.05 m BNF in Toluene; 0.5m or 1m KNO_3 in H_2O.)